Emergency Landing of a Hybrid Electric Tiltrotor After Engine Failure

Jacopo Serafini, Simone Moretti, Giovanni Bernardini, Claudio Pasquali, and Giulio Avanzini

***Abstract*— Due to the increase in short-range air mobility, tiltrotors are expected to get a market share in civil operations. Concomitantly, the need to reduce pollutants and noise emissions requires adopting innovative propulsion, but full-electric tiltrotors are not a feasible solution yet. A series-hybrid retrofit of the XV-15 is thus proposed. An emergency landing procedure is suggested for the critical case of engine failure when batteries are fully discharged. Aircraft rotors act as wind turbines, extracting power during the glide, and recharging the batteries for electrically powered conversion and landing. The propulsive retrofit of the XV-15 shows that current battery technology is not mature to make it a viable solution, and a complete vehicle redesign would be required, exploiting other side-effects of hybrid propulsion on aerodynamic performance. However, the improvement in the performance of the accumulators in the next decade can significantly modify this scenario. The proposed emergency landing procedure consists of a constant-speed descent after and before a constant altitude deceleration. The analysis shows that the optimal descent speed is between 55 and 60 m/s. The limited variation of rotor collective pitch and glide path angle should make performing the emergency sequence relatively easy for the pilot.**

***Index Terms*— Emergency procedure, flight mechanics, hybrid tiltrotor.**

I. Introduction

SINCE the introduction of jet engines, air transport has developed considerably, doubling its volume approximately every 20 years [1]. For this reason, its environmental impact has gained more and more attention. Switching to electric propulsion is being considered one of the most promising ways to decrease this impact, as demonstrated by a growing interest from manufacturers, regulatory offices, and the aviation community [2], [3], [4], [5], [6].

However, despite their quick improvements, batteries and fuel cells are not yet able to guarantee the required performance for conventional aircraft missions [7], [8], [9], [10], [11], [12], [13], [14], although analyses suggest that all-electric aircraft are going to be available in a few years for specific operations [15]. As an intermediate, short-term step, hybrid-electric propulsion may provide some benefits [16], [17], [18], notably without the need for complex modifications to airport services such as fuel delivery: a decrease of pollutants and greenhouse gas emissions; a reduction of noise [19]; an overall increase in flight operations safety, thanks to the superior reliability of electric elements, with a reduction of maintenance costs [20], [21]; and design flexibility enabled by distributed propulsion and very high acceleration capabilities.

However, the main driving factor for the transition to this new class of propulsion systems remains the increasing environmental impact of aircraft operations. Indeed, forecasts indicate that in 2050, the share of global CO_2 emissions associated with the aeronautical sector may reach the value of 10%, starting from the current value of about 2.5% [22] (3.6% considering EU28 market [23]), or even grow up to as much as 25%, if other industries will reduce their carbon footprint [24], [25]. Considering a transition to electric or hybrid-electric propulsion, one can limit such an increase to 5% [26].

At present, land transport is still far more convenient for regional and intercity transport, as airports must be often located far from urban centers due to noise impact. Hybrid electric (and—further in the future—fully electric) aircraft can mitigate this problem, connecting with point-to-point route centers poorly connected by road and rail infrastructures. Vertical takeoff and landing (VTOL) aircraft require vertiports that are much less soil-consuming than airports. Finally, the emerging niche of Urban Air Mobility can be a safe and efficient mode of passenger and cargo transport in metropolitan areas [27], reducing travel time in many services such as airport shuttle, taxi, delivery, ambulance, police, and other first-response public services, for which the use of VTOL aircraft is mandatory.

Tiltrotors combine the VTOL and hover flight capabilities of helicopters with performance in terms of speed, range, endurance, and ceiling altitude approaching those of conventional turboprops. Although their use is currently limited to military operations, the concept of Civil Tiltrotor (CTR) was investigated [28] with different proposals, like the in-production AW609 and the Next Generation CTR concept studied in the CleanSky2 project.[1] A concept for a large CTR (LCTR) was also developed as part of the NASA Heavy Lift Rotorcraft Systems Investigation, in which this concept was shown to have the best cruising efficiency, the lowest weight,

Manuscript received 26 May 2023; accepted 12 August 2023. Date of publication 21 August 2023; date of current version 18 June 2024. *(Corresponding author: Jacopo Serafini.)*

Jacopo Serafini, Simone Moretti, Giovanni Bernardini, and Claudio Pasquali are with the Department of Civil, Computer Science and Aeronautical Technologies Engineering, Rome Tre University, 00146 Rome, Italy (e-mail: serafini@uniroma3.it).

Giulio Avanzini is with the Department of Engineering for Innovation, University of Salento, 73100 Lecce, Italy.

Digital Object Identifier 10.1109/TTE.2023.3306456

[1] https://clean-aviation.eu/next-generation-civil-tiltrotor

and the lowest cost compared to other rotorcraft configurations examined [29].

As far as the application of CTRs for commercial transport is concerned, this class of aircraft is expected to alleviate the congestion of major airport hubs, reducing delays and increasing passenger throughput capacity [28], thanks to their ability to conduct runway independent operations (RIOs) [30], and provided that tiltrotors can travel trajectories that are unavailable to fixed-wing aircraft, performing the so-called noninterference operations (NIOs) [30]. However, although the use of CTRs does not worsen the current situation regarding fuel consumption and noise with respect to conventional aircraft [28], the increase in air traffic volume would worsen aviation's overall impact, especially in urban areas. Therefore, using electric or hybrid electric propulsion for this aircraft category is fundamental for their future use.

Moreover, the advantages of this type of propulsion go beyond the abatement of emissions and noise. For example, the shift to electric motors eliminates various problems related to the lubrication of traditional tiltrotor turboshaft [31]. An even greater advantage lies in eliminating the mechanical transmission connecting the two turboshaft engines to guarantee operations in one-engine-inoperative (OEI) conditions. This system has implications on the wing structure of tiltrotors, which notoriously has a reduced span and a high thickness, the latter of the order of 20% of the chord, leading to a pronounced increase of drag and, therefore, reduction of aerodynamic efficiency. Electric or hybrid electric propulsion allows for total elimination of this complex transmission system by replacing it with a system of redundant cables [32], ensuring a reduction in weight and complexity of the aircraft, as well as an improvement of its aerodynamic efficiency. Furthermore, electric motors are drastically more reliable than gas turbines, reducing the possibility of failures and, therefore, OEI conditions.

Considering series-hybrid aircraft, the most likely propulsion faults are the internal combustion engine failure, or a fuel system failure (including lack of fuel and fuel contamination). Although these aircraft are inherently safer than traditional ones due to the presence of batteries that can power an emergency landing [33], the batteries reach the minimum state of charge at some point during the flight. This typically happens after a climb, during which the supplementary energy stored in the battery pack has been used as an auxiliary source. In the case of a failure at that point, the hybrid aircraft is forced to glide and then land. Also, in this case, the presence of a battery pack on-board the aircraft increases the safety of the emergency procedure if the decelerated descent is used to recharge the batteries, allowing for an electrically powered landing.

Tiltrotors are well suited for this type of regenerating emergency procedure for two reasons. First, the rotors are large enough to provide acceptable windmilling performance. Second, the capability of performing a vertical landing increases the possibility of having a suitable landing spot in the range, even if the latter is reduced by the increase of flight descent angle necessary to transform part of the potential and kinetic energy into chemical energy in the batteries. This article first reports the hybrid retrofit process of the Bell XV-15. Then, an energetic model for evaluating the performance of the emergency procedure is proposed and applied.

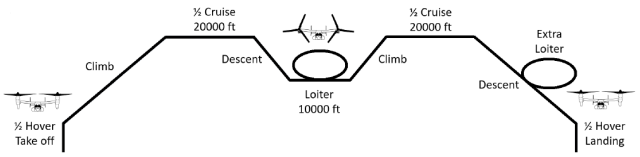

Fig. 1. Mission profile.

II. XV-15 Tiltrotor Retrofit

In this section, the sizing procedure of the XV-15 retrofit is outlined. The sequence of steps described below is implemented within an iterative procedure needed because the fuel consumption of the turboshaft depends on the required power for flight, which in turn depends on the weight of fuel burned during the flight up to that point.

A. Mission Profile

The typical mission of the XV-15, reported in [34] and sketched in Fig. 1, consists of the following phases: 1) vertical take-off followed by a hovering/vertical climb and a conversion phase from helicopter mode (HM) to aircraft mode (AM); 2) climb to the cruise altitude of 20 000 ft; 3) first half of the cruise segment; 4) descent to an altitude of 10 000 ft; 5) loiter at best endurance speed; 6) climb to cruise altitude; 7) second half of the cruise segment; 8) descent to sea level; and 9) vertical landing preceded by a conversion phase from AM to HM and a hovering phase. Regulations [35] require to consider a further loiter phase during the final descent for emergency reasons (e.g., related to particular air traffic or meteorological conditions) or alternatively the continuation of the flight to an alternate airport. Therefore, an additional fuel quantity for flying 30 min is considered.

Following [34], the overall duration and range of the mission have been set to 114 min and 298 nautical miles, respectively. Note that the two conversion phases have been embedded in the HM phases, as the single conversion requires a total time slightly above 10 s, as reported in [36].

B. Selection of the Propulsion System

A series-hybrid electric propulsion system has been chosen for the XV-15 retrofit, being the most suited for multipropeller aircraft and, therefore, also for the twin-rotor configuration of a tiltrotor. It has the advantage of removing the turboshaft engines from the nacelles, eliminating all the problems related to the operation of these engines when tilted (e.g., lubrication). This also allows the nacelle lightening and the removal of the shaft passing through the wing, with the related possible improvements on the wing structure and aerodynamics. The propulsion system proposed in this work is sketched in Fig. 2.

It consists of five branches which are connected through an electrical node: 1) the power generation system (PGS) branch, which includes the PGS consisting of the turboshaft

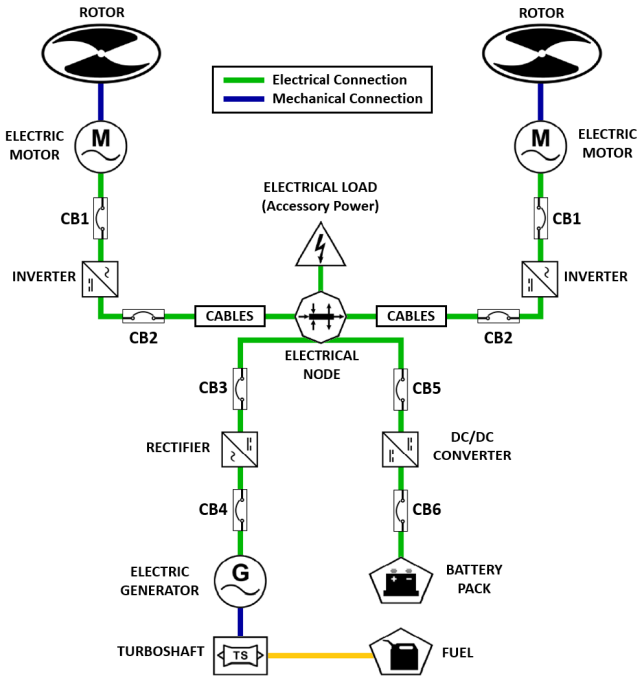

Fig. 2. Scheme of the propulsion system considered for the retrofit operation.

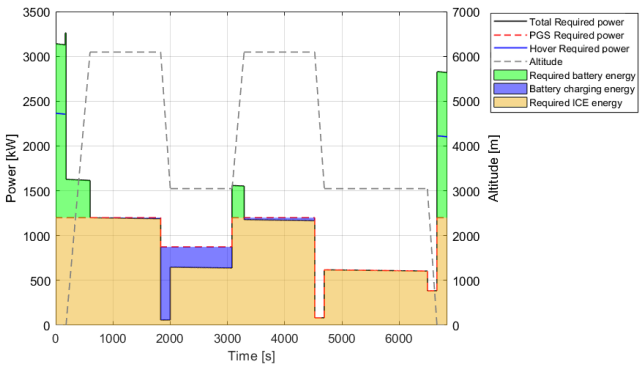

Fig. 3. Required power and power management strategy.

engine(s), the electric generator(s), and the ac/dc rectifier(s); 2) the battery branch, which extends from the battery pack to the electrical node (including the dc/dc converter); 3) the two rotor branches, that are two identical branches extending from the electrical node to the aircraft rotors (including the cables system and the dc/ac inverters); and 4) the accessory branch, which represents the connection between the electrical node and the on-board systems of the aircraft (not described in detail, whose presence is taken into account through the required accessory power).

The propulsion system is sized as the PGS delivers the power for the cruise flight and the onboard systems. In the remaining high-power flight phases (climbs and HM phases), the batteries supply the required extra power, whereas in lower power flight phases (descent and loiter, as well as partly during cruise, thanks to the reduction in required power associated with fuel consumption), the batteries are recharged by the PGS.

C. Required Power Evaluation

Once the mission profile is defined, the required power for each mission leg is evaluated, as shown in Fig. 3 with the black solid line. This figure shows that the HM phases have the highest power demand, followed by the two climb phases in airplane mode. The minimum power is required during the descent phases and the maximum power peak (although of short duration) is required for the conversion phase from HM to AM.

The electrical node, having input powers from the PGS and the batteries and output power for both accessory (necessary for the onboard systems of the aircraft) and propulsive (sent to the two rotors) systems, is characterized by the balance equation

$$P_{\mathrm{PGS}} + P_{\mathrm{BAT}} = P_{\mathrm{ACC}} + 2\,P_{\mathrm{PROP}} \tag{1}$$

where the accessory power is assumed constant and, following [32], estimated as $P_{\mathrm{ACC}} = 49.2$ kW. Furthermore, the power indicated as P_{PROP} represents the power at the "rotor level", increased for the "branch efficiency" (i.e., the efficiency of all the elements between the rotor and the electrical node). Fig. 3 also illustrates the power management strategy actuation through the areas filled in orange, blue, and green, which represent, respectively, the energy provided by the ICE for flight, recharging batteries, and the extra power provided by batteries for high-power phases, respectively. The red dashed line represents the overall power delivered by the ICE during the flight. Note that, during the second part of the flight, the batteries are not recharged since they have already reached their maximum charge level.

D. Specific Fuel Consumption

Like a conventional propulsion aircraft, the series-hybrid version of the XV-15 benefits from a gradual weight loss due to fuel consumption. The specific fuel consumption (SFC) during the different mission phases is evaluated using the regression model proposed in [37]. This model is based on the SFC values of several existing turboshaft engines and expresses the SFC as a function of the engine size, altitude, forward speed, and partial loading. Note that the functioning of the turboshaft engine at a little-varying operating point greatly improves its efficiency. Thus, it reduces the mean SFC by about 17% with respect to the standard XV-15.

E. Sizing Methodology and Power Management

The electric generator, the electric motors, and the power converters are sized using specific power, defining their mass as follows:

$$M_e = P_{\mathrm{out}}/p_e \tag{2}$$

where M_e indicates the element mass, p_e its specific power in [kW/kg], and P_{out} represents the power provided by the element, taking into account its efficiency, based on the current technological level.

The masses of the turboshaft engine and the circuit breakers are evaluated by using the approach proposed in [38] and [39]:

$$M_{gt} = 0.9594\, k_{gt}\, (P_{shaft,gt})^{0.7976} \quad (3)$$

$$M_{IGBT} = (1.6 \cdot 10^{-4}\, P_{IGBT}) + 0.6. \quad (4)$$

In this equation, the mass of the turboshaft engine (M_{gt}) depends not only on the power but also on the parameter k_{gt}, which indicates a technological factor of the gas turbine that can be used to account for expected improvement in turbo machinery technology [38] (assumed in this work of unitary value). Furthermore, the mass of the circuit breakers (M_{IGBT}) refers to the use of the so-called solid state power controllers (SSPCs), widely used in the aeronautical sector for high voltage and high power applications, which are usually realized through the use of insulated gate bipolar transistor (IGBT) [40].

Since the two branches of the propulsion system connecting the rotors to the electrical node manage the same power (i.e., half of the total required power), it is necessary to size only one of them, doubling the mass obtained. The sizing process considers that the output power of each electric motor is given by the maximum power of the single rotor. It corresponds to the peak reached during the conversion phase from HM to AM, reduced by the accessory power. Once the two propulsive branches have been sized, considering the power splitting and knowing that the power of the PGS, P_{PGS}, equals the power at the beginning of the cruise (see Fig. 3), the power of the batteries is evaluated

$$P_{BAT} = 2\, P_{PROP} - P_{PGS}. \quad (5)$$

The knowledge of P_{PGS} allows sizing the elements belonging to the PGS branch (from the electrical node to the turboshaft motor) while P_{BAT} allows sizing the elements of the battery branch. Note that the value assumed by the P_{BAT} power does not coincide with the power delivered by the batteries, as it is necessary to pass through the dc/dc converter and the two circuit breakers present on the considered branch.

F. Battery Sizing

The batteries are sized in terms of power and energy, considering the system-level values for the specific power and energy. Then, the maximum mass value among the two is chosen for the weight evaluation. In this work, two types of battery are considered: lithium-ion (LiB) and lithium-polymer (Li-po). Table I presents the current (2020/2021) values of specific power and energy. Table II reports the values estimated for 2035 as reported in [41]. It is worth noting that recently Amprius Technologies announced the commercialization of a 500 Wh/kg Li-Ion cell which is almost twice the value obtained by current state-of-the-art cells [42].

Although promising, LiS and LiO_2 are excluded due to the fact that these batteries are currently at a lower technological level than the other two. With the current technology, Li-po batteries are the most convenient in weight, corresponding to 1460.49 kg (to comply with the most stringent energy requirement). Nevertheless, the mass of the batteries would already exceed the subtracted mass (SM) of 1136.3 kg, which represents the total mass of the elements removed from the original configuration of the XV-15 (see Table III).

TABLE I
BATTERY PARAMETERS WITH CURRENT TECHNOLOGY (2020/2021)

Battery type	Specific Power [W/kg]	Specific Energy [Wh/kg]
Lithium Ion	1365 [44]	210 [44]
Lithium Sulfur	1000 [45]	650 [45]
Lithium Air	1000 [45]	610 [44]
Lithium Polymers	5860 [42]	120.2 [42]

TABLE II
BATTERY PARAMETERS WITH FUTURE TECHNOLOGY (2035)

Specific Power [W/kg]	Specific Energy [Wh/kg]
19000 [42]	1021.5 [42]

TABLE III
SUBTRACTED MASSES (DATA FROM [34])

Elements	Mass [kg]
Engine installation	492.2
Air induction	7.7
Exhaust system	7.7
Lubrication system	10
Fuel system	87.1
Engine controls	18.6
Starting system	43.5
Gearboxes	445.9
Interconnect drive	23.6
Total Subtracted Mass	1136.3

To reduce the weight of the batteries, a design exploiting a double battery pack, one consisting of Li-po batteries and the other of LiB batteries (see Fig. 4), is proposed. The following observations drive this solution: 1) Li-po batteries can easily manage power peaks, as they have high specific power; and 2) LiB batteries, on the other hand, can be used for the prolonged phase at low power as they have high specific energy.

With this solution, both power and total energy are split between the two battery packs, with the optimal split shown in Fig. 5. Such a design identifies a mass for the Li-po and LiB batteries equal to 670.13 and 453.2 kg, respectively, for a total mass of 1122.44 kg, which compared with the mass obtained for Li-po batteries alone leads to a 23.14% reduction, resulting in a saving of 141.79 kg. Fig. 6 shows this result. However, even with this redesign philosophy, the mass of the batteries is only 13.86 kg lower than that of the SM. So, even in this case, the subtracted masses are almost completely recovered with the mass of batteries alone. Instead, considering the future technology levels hypothesized in [41], the overall battery mass drops to 171.83 kg, with a consistent saving (about 1 ton).

G. Thermal Management System Sizing

A detailed sizing of the TMS is very complex, as it is linked to the type of elements making up the propulsion system, and it affects not only the weight of the aircraft but also its aerodynamics, for example, due to the presence of air heat exchangers that require appropriate intakes. Following [45], a rough estimation of the TMS mass is provided by using the specific power value considered valid for several

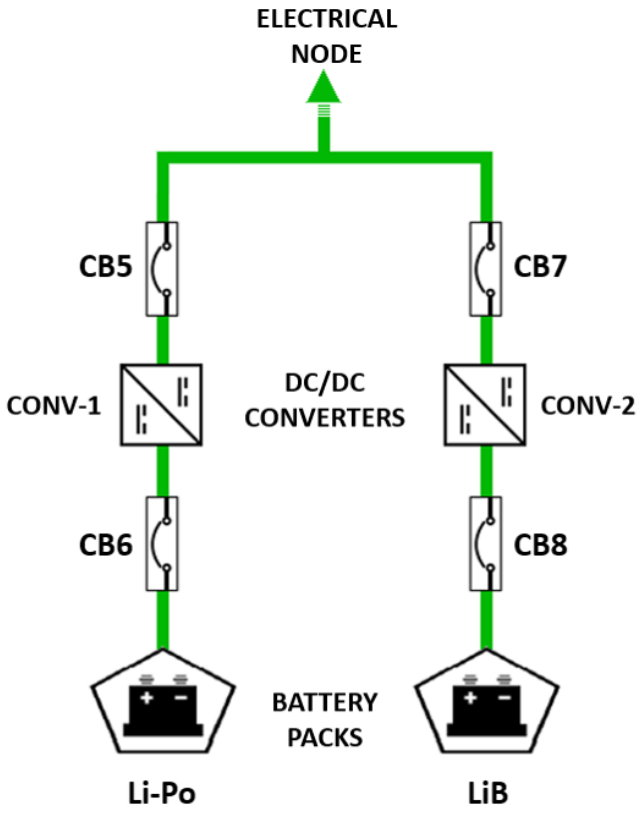

Fig. 4. Double battery branch scheme.

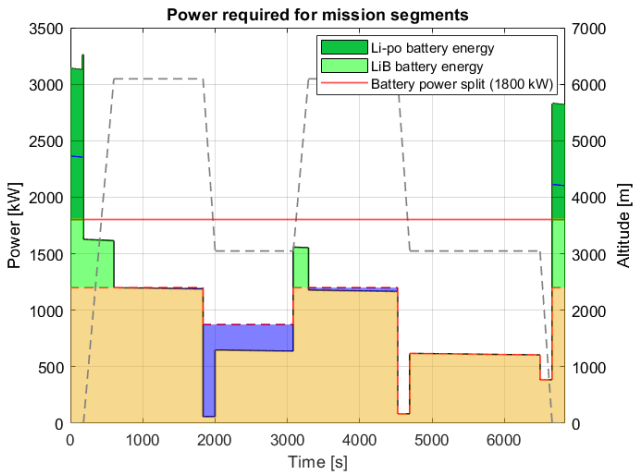

Fig. 5. Double battery optimized power and energy split.

more-electric aircraft (MEA) and therefore assumed valid also for this work, corresponding to $p_{\text{TMS}} = 0.68$ kWth/kg. The evaluation of p_{TMS} requires the knowledge of the thermal power developed by the propulsion system. This power can be computed from the efficiency and input power of each element of the propulsive system. When high-temperature superconductors (HTSs) are used in place of metallic cables, it is also necessary to estimate the weight of the cryogenic cooler, for which the weight can be estimated following the suggestions contained in [46].

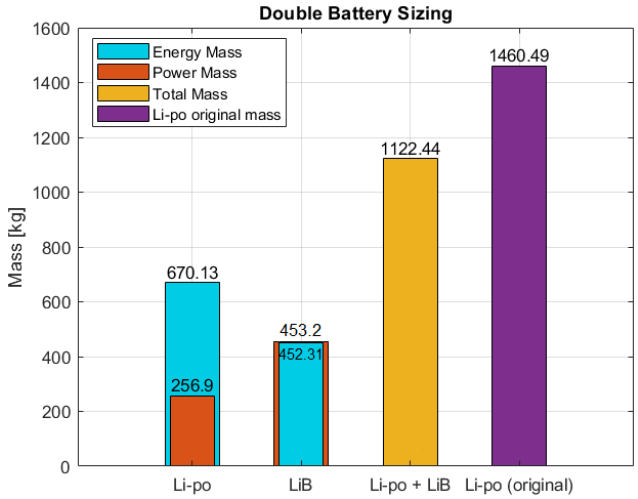

Fig. 6. Comparison between single and double-pack battery mass.

H. Fuel Mass Evaluation

The fuel required for the mission is evaluated by adding the contributions of fuel burned in each single mission leg. They are obtained as the time integral of the product between each mission segment SFC and power.

Note that the fuel masses used in the sizing process are congruent only if the MTOMs of the hybrid electric XV-15 would result equal to the original DTOM value, which has been used to calculate the necessary power of each mission leg. In all other cases, either the mission should be modified (e.g., shortened), or a modification of weight (e.g., an increase of the batteries specific energy) should be considered.

I. Overall Weight Estimation

In [47] provides an overall empty mass (including liquids except for fuel) of 4631 kg. It is then possible to proceed with the definition of the new partial empty mass (PEM) of the hybrid electric version of the XV-15 (in the following indicated as HE XV-15) as the difference between the overall empty mass and SM (3432.7 kg). Once the PEM has been defined, the next step is the evaluation of the new propulsion system mass (PSM), for which the following considerations are made.

1) The masses of the propulsion system will be distinguished between current and future battery technology. With regard to current technology, a double battery branch configuration is used, while the single battery branch approach is used for future technology.
2) Three cases are distinguished for the cabling system: copper cables, aluminum cables (both characterized by the same TMS), and HTS cables with the relative TMS (which also includes the cryogenic cooling system).

Following a standard approach, the preliminary sizing can be defined with the following expression:

$$\text{MTOM}_{\text{new}} = \text{PEM} + \text{PSM} + M_{\text{fuel}} + M_{\text{payload}} + M_{\text{crew}} \quad (6)$$

where, apart from the PEM and the PSM, the other masses will be considered as follows.

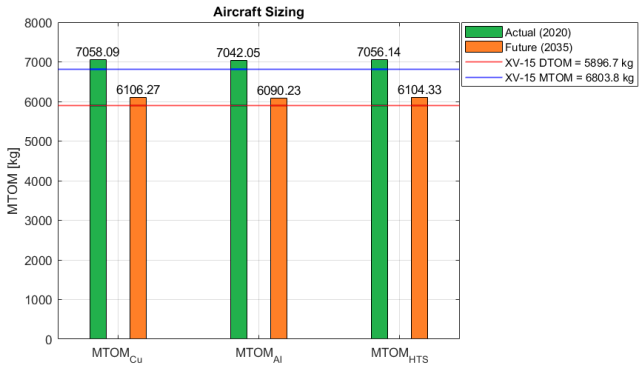

Fig. 7. MTOM after retrofit.

1) For the crew, consisting of two pilots, [47] indicates 90 kg for each of them.
2) For the payload, [47] provides the indication of 407 kg consisting mainly of research instrumentation.

The result for the new MTOM of the aircraft is shown in Fig. 7. The difference in mass related to the wiring systems is minimal, with maximum variations of about 1%. Concerning the difference associated with the technological levels of the batteries, an average reduction of 13% can be achieved by passing from the current technology to the hypothesized future one.

Finally, it is essential to note that all the overall masses obtained with the current technology are higher than the original value of the Design Take-Off Mass of the XV-15 (red horizontal line in the figure) and Maximum Take-Off Mass (blue horizontal line in the figure). Considering the 2035 technology level, the weight of the retrofit XV-15 would drop below the original MTOM but would remain slightly higher than the original DTOM. However, two aspects should be considered. First, no improvement has been considered on the technological level of the other components. Second, and more importantly, the reduction of wing weight and the improvement of wing aerodynamic efficiency (up to about 40%, considering parasite and induced drag) due to the absence of the shaft leads to a reduction of both aircraft weight and required power (and thus battery weight). The exact amount of these weight savings requires a completely new redesign of the aircraft rather than a simple retrofit. However, the above analysis suggests the feasibility of a hybrid tiltrotor in a few years.

III. Fault Occurrence and Emergency Procedure

The energy management strategy for power partition between the turboshaft-generator unit and the batteries in the proposed tiltrotor retrofit induces the presence of an energetically critical condition for the aircraft at the beginning of the first cruise segment when the batteries are at their minimum state of charge after the previous power intensive phases of vertical take-off, conversion, and climb.

Therefore, in the hypothesis of a failure of the turboshaft engine or the fuel system at the end of the climb, the aircraft would remain without propulsive power during the descent and - more importantly - at landing. Note that landing should be performed in either AM or in HM. In the first case, two aspects are critical: 1) a large amount of runway-like obstacle-free space is necessary for decelerating the aircraft after touchdown and 2) current tiltrotors are not able to land in AM due to geometric constraints. Studies for tiltrotor with smaller rotors capable of A/C mode landing have been conducted in the past [48]. At the same time, landing in HM is even more difficult provided that: 1) some residual energy is required for tilting the nacelles upward; 2) the final approach should be performed after transitioning from a fixed-wing gliding flight to an autorotation mode (a maneuver far from trivial, although already performed [49]; 3) the touchdown in autorotation still requires a considerable amount of obstacle-free space, provided the rotational kinetic energy of the prop-rotors is unlikely to be sufficient for fully stopping the vehicle before touchdown; and 4) finally landing in autorotation is even more difficult for a tiltrotor than for a conventional helicopter, due to the reduced aerodynamic performance.

Developing an appropriate emergency landing procedure is thus a relevant issue for vehicle safety. This procedure aims to recharge the batteries with sufficient energy for performing a short electrically powered vertical emergency landing, including the conversion from airplane to HM. Batteries are recharged, assuming that electric motors can be used as generators, receiving mechanical power from the rotors used as the prime mover in a windmilling condition. Thus, the gliding descent performed in AM after the failure is also intended as a regenerative descent and braking phase, transforming part of the potential energy of the tiltrotor into chemical energy stored in the batteries.

An emergency procedure for a similar scenario, after thermal engine failure for a helicopter featuring hybrid-electric propulsion, is investigated in [41], where a sufficient battery charge for managing the final touchdown phase after an autorotation descent was assumed. In the present work, a more demanding situation is considered, where the battery charge is at a minimum, not allowing for completing an electrically powered landing maneuver.

The procedure is divided into a sequence of six steps.

1) Nonregenerative deceleration at the cruising altitude at which the failure occurs (assumed equal to 20 000 ft), down to a certain value of speed.
2) Gliding flight, down to an altitude of approximately 1000 ft above sea level, during which the batteries are recharged.
3) Nonregenerative deceleration at conversion altitude down to conversion speed.
4) Conversion from AM to HM, which takes approximately 12 s, around an altitude of 1000 ft.
5) Autorotation for approximately 2/3 of the remaining altitude after conversion (650 ft, that is, 200 m).
6) Use of the energy stored in the batteries for conversion, a powered 350 ft (approximately 100 m) descent and a short hover phase for a safe vertical landing.

Please note that in the following analysis, the procedure feasibility is evaluated only by means of an energy budget, without going into the details of the transitions from one phase

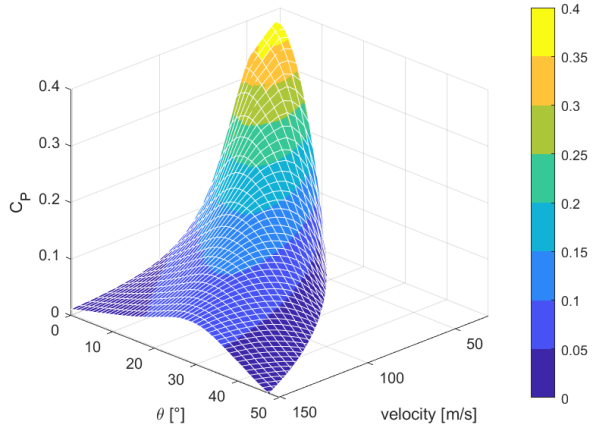

Fig. 8. Power coefficient map.

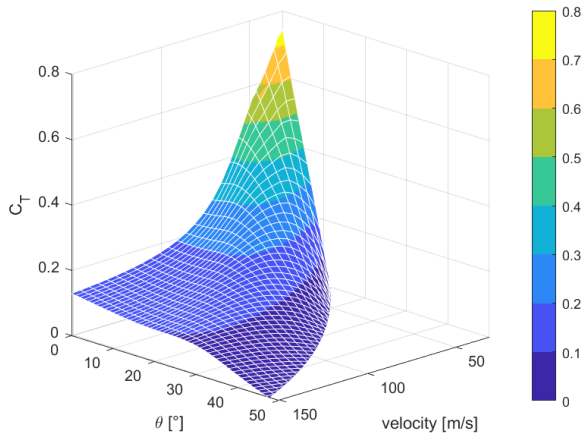

Fig. 9. Thrust coefficient map.

to the following one. Also, for the sake of simplicity, the second phase is included in the terminal section of phase 1, provided that its duration of 12.6 s for the Bell XV-15 is small compared to that of the following gliding phase.

IV. Regenerative Maneuver

A. Windmilling Performance

The regenerative process used for battery recharge during the glide by means of the rotors in windmilling conditions is analyzed on the basis of a standard approach in wind turbine analysis. The aerodynamic analysis of the XV-15 rotors in windmilling mode has been performed using QBlade software [50], which provides an estimate of generated power and thrust coefficients as a function of flow mean speed through the disk, V, and collective blade pitch angle, θ, for a fixed rotor angular speed. The results can be expressed in terms of nondimensional power and thrust coefficients, namely

$$C_P(\theta, V) = \frac{P(\theta, V)}{0.5\rho A V^3}, \quad C_T(\theta, V) = \frac{T(\theta, V)}{0.5\rho A V^2} \tag{7}$$

where ρ is air density and A is the rotor disk area. QBlade uses a Blade-Element Momentum Theory corrected with tip and root losses. It can also perform Lifting Line Free-Vortex Wake analysis, where the wake is modeled through Lagrangian vortex elements. Still, the first approach was selected as a compromise between acceptable accuracy for the purposes of the present analysis and a reduced computational cost.

Figs. 8 and 9 show power and thrust coefficient maps resulting from the QBlade analysis, in the range of mean airflow velocities and blade pitch angles of interest for this problem. From the point of view of the windmilling performance, a maximum is attained for the lowest airflow velocity, coherently with the standard optimal range of tip speed ratio $\Omega R/V_\infty$ for windmilling rotors of the same solidity.

B. Power Balance in Gliding Flight

The power balance equation during gliding flight can be written in the form

$$mg\dot{h} + mV\dot{V} = -(DV + 2TV) \tag{8}$$

where

1) The first term on the left-hand side represents the time derivative of aircraft potential energy.
2) The second term on the left-hand side is the time derivative of vehicle kinetic energy, which is equal to zero if the regenerative descent is performed at a constant speed.
3) The first term on the right-hand side is parasite power of aircraft, given by the product of drag times airspeed
$$DV = \frac{1}{2}\rho V^3 S C_D \tag{9}$$
where drag coefficient C_D is the sum of parasite drag coefficient C_{D_0} and induced drag $k\,C_L^2$; hence, C_D in steady glide depends on aircraft weight, W, according to the equation
$$DV = \frac{1}{2}\rho V^3 S\left[C_{D_0} + k\left(\frac{2W}{\rho V^2 S}\right)^2\right]. \tag{10}$$
4) The second term on the right-hand side represents power associated with the axial force (negative thrust) generated by the rotors in windmilling conditions.

C. Evaluation of Total Energy Recovered

If the total loss of altitude is divided into N intervals, (8) can be integrated over each interval considering ρ approximately constant, equal to the value at its midpoint according to the international standard atmosphere (ISA) model.

A potential energy conversion efficiency can be defined as follows:

$$\eta(\theta, V) = \frac{2P}{DV + 2TV} \tag{11}$$

for each interval of altitude, which represents the fraction of potential energy lost per unit time, with $DV + 2TV = -mg\dot{h}$, from the power balance, converted into shaft power. An increase in η results in a higher generated energy, at the expense of distance traveled (steeper descent).

The regenerated energy in the ith interval ΔE_{e_i} is calculated as follows:

$$\Delta E_{e_i} = \eta\,\eta_{\text{tot}}\,mg\Delta h_i \tag{12}$$

where η_{tot} is the overall efficiency of mechanical transmission and electric powertrain, which consists of a generator, energy converter, cables, safety circuit breakers, and batteries. A value $\eta_{\text{tot}} = 0.9$ is here assumed. The overall value of regenerated energy is then simply evaluated as $E_e = \sum_{i=1}^{N} \Delta E_{e_i}$ from cruise to conversion altitude.

A limit is enforced on maximum power $P_{\max}$ that can be generated from each electric motor, when it operates as a generator, assuming that this limit equals the maximum power that can be supplied by the electric motor in its normal operating mode (i.e., 3 MW). Considering the battery sizing proposed above, this corresponds to a 17C charge rate, a quite high but acceptable value for an emergency procedure, especially when the battery is at the lowest charge. If the battery cannot accept all the power, the PGS group can absorb part of the exceeding power, making the turboshaft spin idle. At the same time, future batteries characterized by a significantly higher admissible C-rate (like solid-state ones) are expected to mitigate the problem.

Therefore, all cases with power values exceeding 3 MW are discarded as nonfeasible since this condition would imply that the excess of aerodynamic torque drives the angular rotor speed beyond its nominal value. Similarly, cases with a negative instantaneous power obtained after subtracting drag losses are discarded, since this would decrease rotor kinetic energy. In this work, the rotor speed is assumed constant, although other works investigated the advantages of variable-speed rotors [51]. These advantages may be fully exploited by using electric or hybrid propulsion, which removes the need for a complex multiple-speed transmission. Finally, a limit of $-20°$ has been imposed on the flight path angle to avoid too steep descents.

Results regarding regenerated energy as a function of descending strategy are presented and discussed in Section V. Available hovering time after conversion and autorotation approach is also reported to provide a practical guideline. This time corresponds to the time available for the final emergency landing, and it is evaluated as follows:

$$t_H = E_e \big/ P^r_{H,\text{em}} \tag{13}$$

where $P^r_{H,\text{em}}$ is the required power for the emergency hover phase, evaluated at battery terminals, considering aircraft mass at the time of failure, namely

$$P^r_{H,\text{em}} = \left(P_i + P^h_0\right) \big/ \eta_{\text{tot}}. \tag{14}$$

Induced power

$$P_i = k_i \, T \, v_i \tag{15}$$

is calculated by means of momentum theory as the product between rotor thrust, $T \approx W$, and induced speed at rotor disk plane, $w_i = [T/(2\rho A)]^{1/2}$, in hover condition, $V = 0$ [52]. A correction factor $k_i = 1.05$ [53] accounts for the effects of rotor tip losses, nonuniform inflow, wake swirl, nonideal wake contraction, and the finite number of blades [26]. The second contribution in (14), P^h_0, represents rotor profile power in hovering conditions, which is required to overcome blade profile drag. In the framework of blade element theory, P^h_0 is

$$P^h_0 = \rho \, A \, V^3_{\text{tip}} \left(\frac{\sigma \, C_{d_0}}{8} \right) \tag{16}$$

where blade tip speed is $V_{\text{tip}} = \Omega R$, $\sigma = N_{\text{bl}} A_{\text{bl}}/(\pi R^2)$ is rotor solidity (that is, the ratio between total blade area and rotor disk area), and C_{d_0} is blade section average drag coefficient.

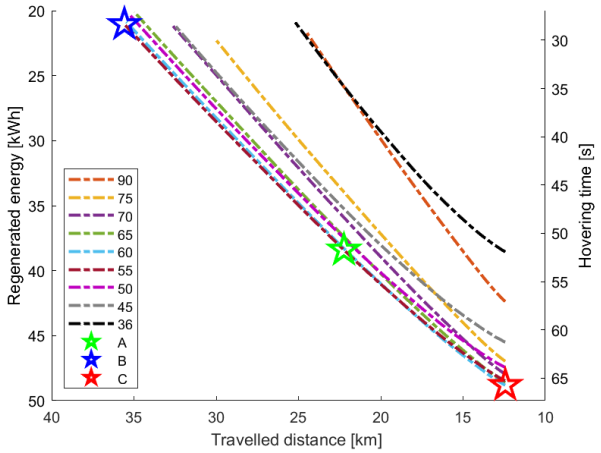

Fig. 10. Pareto front of optimization problem for different descent velocities.

V. Numerical Results on Emergency Maneuver

The analysis discussed above allows one to evaluate the extracted energy, delivered to the battery pack, and the resulting hover time, together with the traveled distance during the regenerative descent as a function of flight velocity at which the maneuver is performed. First, Fig. 10 shows the variation of regenerated energy versus distance traveled for different descent airspeed. The results are obtained from the integral over the whole descent path of the best solutions for each altitude interval of the objective function $J_i = (1-\alpha)\,\eta_i - \alpha\gamma_i/\gamma_{\max}$, with the maximum value of admissible glide angle $\gamma_{\max} = 20°$. The envelope of the curves determines the Pareto front for the multiobjective optimization problem in terms of maximum regenerated energy and distance traveled. The available energy at the end of the descent corresponds to an equivalent hovering time, reported in the secondary axis, on the right of the plot.

The optimal range of velocity lies between 55 and 60 m/s, with the former providing optimal results in terms of regenerated energy and the latter the longest distance traveled. The utopia point is obtained as the point (outside of the Pareto front) with coordinates equal to the optimal values for the two performance indexes. Three points are then considered for the following analysis. The first one (A) is the point of minimum distance from the utopia point on a plane with horizontal and vertical axes normalized with respect to the distance traveled in nonregenerative descent at best glide ratio and total loss of potential energy during descent, respectively. Point A can be considered as the "best of the bests" and it lies on the curve derived for an airspeed equal to 55 m/s. Point B corresponds to the first value of regenerated energy above 20 kWh, which has

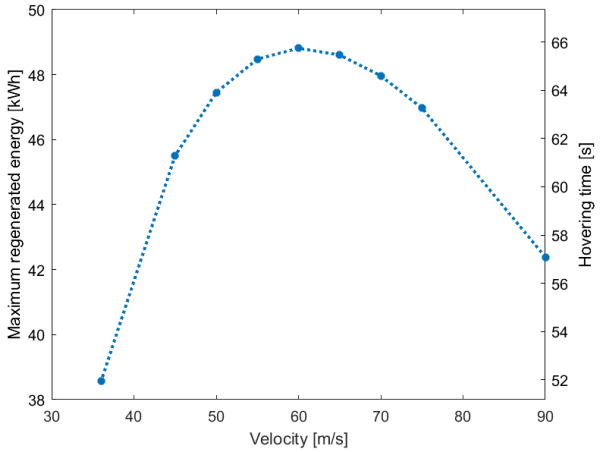

Fig. 11. Maximum regenerated energy as a function of airspeed.

been set as the minimum battery charge sufficient to perform conversion and landing safely. This point also lies on the 55 m/s curve, yielding the longest distance traveled. The last point (C) lies on the 60 m/s curve, obtained at the steepest admissible descent angle, providing the maximum regenerated energy (hence, the longest hovering time).

Fig. 11 represents the maximum amount of regenerated energy obtained along the steepest descent. All these values depend on the velocity, assumed constant during the descent. Apparently in contrast with what was shown in Fig. 8, the maximum regenerated energy is obtained for a velocity higher than that expected from the C_P plot. This is due to the fact that, as stated before, the increase of rotor (negative) thrust and aircraft-induced drag causes power losses higher than the gain achieved by the increased power coefficient. Figs. 12–14 show the detailed analysis of the variation of relevant quantities during descent from cruise to conversion altitude for the three maneuvers corresponding to points A, B, and C (units for the x-axis in these plots are reported in the box, as the x-axis is common when the variation of the four quantities as a function of altitude is represented). In all three cases, the variation in descent path angle γ and required collective pitch θ is quite small, thus making the maneuvers relatively easy to perform for the pilot. Regenerated energy and distance traveled curves have a smooth trend, increasing almost linearly with altitude loss.

Finally, Fig. 15 shows how the potential energy conversion efficiency, η, varies with altitude, velocity, and collective pitch angles in the range of its allowable values (whose upper and lower bounds are defined by the red lines). Descending, to maintain the same value of η, it is required to increase the collective pitch monotonically. Furthermore, speed affects the range of allowable values for the collective pitch during the descent. For lower altitudes, the lower limit of collective pitch narrows down due to the increase of thrust for the same pitch value, which causes a quicker increase in descent path angle. For higher velocity, as expected, the graph almost translates to the right due to the change of velocity triangle on the blade.

In order to experimentally test the emergency procedure analyzed above, a preliminary assessment of the windmilling

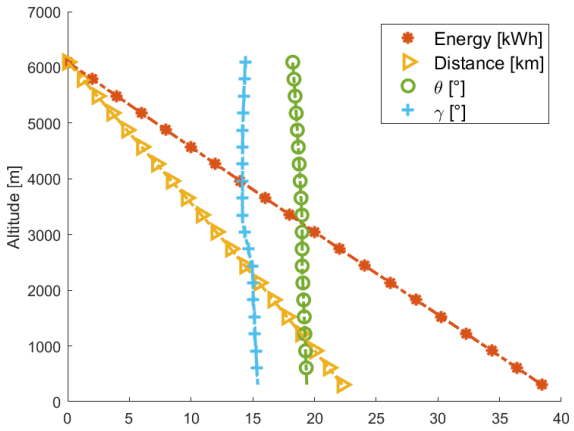

Fig. 12. Regenerated energy, distance traveled, flight path angle, and required collective pitch during descent for A point.

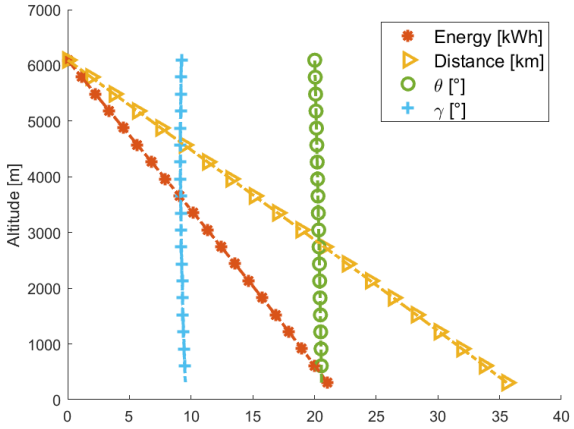

Fig. 13. Regenerated energy, distance traveled, flight path angle, and required collective pitch during descent for B point.

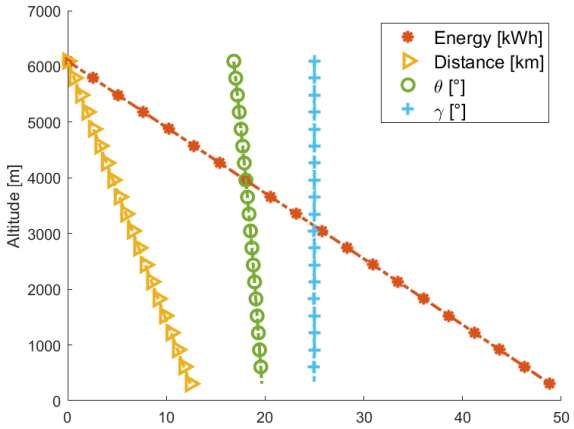

Fig. 14. Regenerated energy, distance traveled, flight path angle, and required collective pitch during descent for C point.

performance of the wing-rotor assembly should be performed. This can be achieved in wind tunnel testing, thanks to the relatively small size of the prop-rotors, with respect to standard wind turbines. The testing should also include bench tests of the electric drive in regenerative functioning, including transient when switching from one mode to another. In addition to in-flight windmilling validation, flight testing should concern

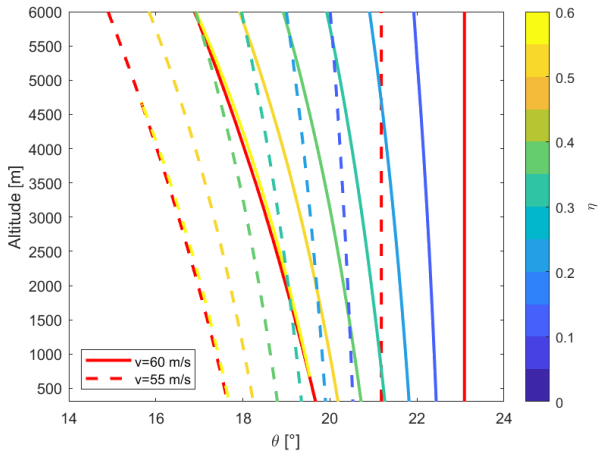

Fig. 15. Region of admissible values of the collective pitch during descent concerning the two velocities of interest. Colored lines are iso-η.

the transitions between different maneuver phases, to highlight possible aeromechanical and electrical issues during the entire emergency procedure. In order to reduce risks within acceptable levels, a preliminary simulation of a complete digital twin (including the physical twin of the electric system and the simulated twin of tiltrotor aeromechanics) should be carried out, including unsteady effects during the whole maneuver.

VI. Conclusion

The retrofit process of the XV-15 to a series-hybrid powertrain has demonstrated that current technology for batteries is insufficient in terms of specific energy and power to design an electrified version of the XV-15 with approximately the same weight. However, battery performance has constantly improved during the last years at a significant rate, which should allow for a feasible retrofit in less than 20 years. Moreover, the electrification of a tiltrotor allows a significant improvement in wing aerodynamic performance and structural weight, which makes weight parity closer. This needs to be quantified in a complete design process.

Batteries simplify the emergency management of a hybrid tiltrotor in case of turboshaft engine failure. However, in the case of depleted batteries at the moment of failure, the authors demonstrated that the tiltrotor gliding might be used as a regenerative phase to allow a powered landing in HM. A simple maneuver consisting of a regenerative descent from cruise to conversion altitude at a constant airspeed (about 55–60 m/s) charges the batteries with sufficient energy, allowing the tiltrotor to perform a powered conversion and landing. The pilot can choose the best trade-off between the opposed goals of traveled distance during the gliding phase and regenerated energy as a function of landing constraints.

References

[1] J.-P. Rodrigue, *The Geography of Transport Systems*. Evanston, IL, USA: Routledge, 2020.

[2] K. Hamilton and T. Ma, "Electric aviation could be closer than you think," Scientific American, Nov. 2020. [Online]. Available: https://www.scientificamerican.com/article/electric-aviation-could-be-closer-than-you-think/

[3] S. Morris, "'Decarbonising aviation': The electric EEL could be the future of flying," The Guardian, Aug. 2021. [Online]. Available: https://www.theguardian.com/environment/2021/aug/24/decarbonising-aviation-the-electric-eel-could-be-the-future-of-flying

[4] N. Rufford, "Are electric planes the future of flight?" The Times, Nov. 2021. [Online]. Available: https://www.thetimes.co.uk/article/are-electric-planes-the-future-of-flight-mvr738dn0

[5] (2021). *Electric Flight—Laying the Groundwork for Zero-Emission Aviation*. [Online]. Available: https://www.airbus.com/en/innovation/zero-emission/electric-flight

[6] (2021). *Electric and Hybrid Aircraft Platform for Innovation (E-HAPI)*. [Online]. Available: https://www.icao.int/environmental-protection/Pages/electric-aircraft.aspx

[7] T. C. Cano et al., "Future of electrical aircraft energy power systems: An architecture review," *IEEE Trans. Transport. Electrific.*, vol. 7, no. 3, pp. 1915–1929, Sep. 2021.

[8] S. Rondinelli et al., "Challenges and benefits offered by liquid hydrogen fuels in commercial aviation," in *Proc. Practical Responses Climate Change Conf.* Barton, ACT, Australia: Engineers Australia, 2014, pp. 216–226.

[9] F. Zhang and J. Maddy, "Investigation of the challenges and issues of hydrogen and hydrogen fuel cell applications in aviation," *TechRxiv*, 2021, doi: 10.36227/techrxiv.14958057.v1.

[10] J. Serafini, M. Cremaschini, G. Bernardini, L. Solero, C. Ficuciello, and M. Gennaretti, "Conceptual all-electric retrofit of helicopters: Review, technological outlook, and a sample design," *IEEE Trans. Transport. Electrific.*, vol. 5, no. 3, pp. 782–794, Sep. 2019.

[11] X.-G. Yang, T. Liu, S. Ge, E. Rountree, and C.-Y. Wang, "Challenges and key requirements of batteries for electric vertical takeoff and landing aircraft," *Joule*, vol. 5, no. 7, pp. 1644–1659, Jul. 2021.

[12] A. Narishkin, E. Ocbazghi, and S. Cameron, "Why electric planes haven't taken off yet," Business Insider, Apr. 2021. [Online]. Available: https://www.businessinsider.com/electric-planes-future-of-aviation-problems-regulations-2020-3?r=US&IR=T

[13] A. Eppinga, "Future of electric aviation: 'Batteries only suitable for small-scale flights,"' Innovation Origins, Aug. 2021. [Online]. Available: https://innovationorigins.com/en/future-of-electric-aviation-battery-only-suitable-for-small-scale-flights/

[14] R. Furchgott, "Can hydrogen save aviation's fuel challenges? It's got a way to go," New York Times, Nov. 2021. [Online]. Available: https://www.nytimes.com/2021/11/15/business/airplanes-hydrogen-fuel-travel.html

[15] T. Bærheim, J. J. Lamb, J. K. Nøland, and O. S. Burheim, "Potential and limitations of battery-powered all-electric regional flights—A Norwegian case study," *IEEE Trans. Transport. Electrific.*, vol. 9, no. 1, pp. 1809–1825, Mar. 2023.

[16] D. P. Decerio and D. K. Hall, "Benefits of parallel hybrid electric propulsion for transport aircraft," *IEEE Trans. Transport. Electrific.*, vol. 8, no. 4, pp. 4054–4066, Dec. 2022.

[17] J. J. Botti, "Hybrid electric aircraft to improve environmental impacts of general aviation," *Bridge*, vol. 50, no. 2, pp. 15–20, 2020.

[18] M. A. Rendón, R. C. D. Sánchez, M. J. Gallo, and A. H. Anzai, "Aircraft hybrid-electric propulsion: Development trends, challenges and opportunities," *J. Control, Autom. Electr. Syst.*, vol. 32, pp. 1244–1268, Jun. 2021.

[19] C. E. D. Riboldi, L. Trainelli, L. Mariani, A. Rolando, and F. Salucci, "Predicting the effect of electric and hybrid-electric aviation on acoustic pollution," *Noise Mapping*, vol. 7, no. 1, pp. 35–56, Jan. 2020.

[20] K. O. Ploetner, "Operating cost estimation for electric-powered transport aircraft," in *Proc. Aviation Technol., Integr., Oper. Conf.*, Aug. 2013, p. 4281.

[21] M. M. Monjon and C. M. Freire, "Conceptual design and operating costs evaluation of a 19-seat all-electric aircraft for regional aviation," in *Proc. AIAA Propuls. Energy Forum*, Aug. 2020, p. 3591.

[22] H. Ritchie, "Climate change and flying: What share of global CO_2 emissions come from aviation?" Our World in Data, 2020. [Online]. Available: https://ourworldindata.org/co2-emissions-from-aviation

[23] EASA. (2022). *European Aviation Environmental Report*. [Online]. Available: https://www.easa.europa.eu/eco/eaer/topics/overview-of-aviation-sectors

[24] H. Ritchie, "Cars, planes, trains: Where do CO_2 emissions from transport come from?" Our World in Data, 2020. [Online]. Available: https://ourworldindata.org/co2-emissions-from-transport?country=

[25] *Energy Technology Perspectives 2020*, IEA, Paris, France, 2020.

[26] A. R. Serrano, "Design methodology for hybrid (VTOL + fixed wing) unmanned aerial vehicles," *Aeronaut. Aerosp. Open Access J.*, vol. 2, no. 3, pp. 165–176, Jun. 2018.

[27] A. Pukhova, C. Llorca, A. Moreno, C. Staves, Q. Zhang, and R. Moeckel, "Flying taxis revived: Can urban air mobility reduce road congestion?" *J. Urban Mobility*, vol. 1, Dec. 2021, Art. no. 100002.

[28] L. Young et al., "Civil tiltrotor aircraft operations," in *Proc. 11th AIAA Aviation Technol., Integr., Oper. (ATIO) Conf.*, Sep. 2011, p. 6898.

[29] W. Johnson, G. K. Yamauchi, and M. E. Watts, "Designs and technology requirements for civil heavy lift rotorcraft," in *Proc. AHS Vertical Lift Aircr. Design Conf.*, 2006, pp. 1–26.

[30] W. W. Chung et al., "Modeling high-speed civil tiltrotor transports in the next generation airspace," Nat. Aeronaut. Space Admin., Ames Res. Center, Washington, DC, USA, Tech. Rep. NASA/CR–2011-215960, 2011.

[31] I. F. Kuhn Jr., "Purebred and hybrid electric VTOL tilt rotor aircraft," U.S. Patent 8 469 306, Jun. 25, 2013.

[32] R. A. Danis, M. W. Green, J. L. Freeman, and D. W. Hall, "Examining the conceptual design process for future hybrid-electric rotorcraft," NASA, Washington, DC, USA, Tech. Rep. CR-2018-219897, 2018.

[33] M. Montazeri-Gh and M. Khasheinejad, "Dynamic modeling and rule-based control design for a hybrid-electrified regional aircraft," *IEEE Trans. Transport. Electrific.*, vol. 8, no. 4, pp. 4140–4147, Dec. 2022.

[34] J. Magee and H. Alexander, "A hingeless rotor XV-15 design integration feasibility study, volume I and II," NASA, Philadelphia, PA, USA, Tech. Rep. NASA-CR-152310, 1978.

[35] *Notice of Proposed Amendment 2016-06 (B)—Fuel Planning and Management*, EASA, Cologne, Germany, 2016.

[36] D. C. Dugan, R. G. Erhart, and L. G. Schroers, *The XV-15 Tilt Rotor Research Aircraft*. Washington, DC, USA: NASA, 1980.

[37] F. Stagliano and M. Hornung, "Impact of novel propulsion system architectures incorporating diesel engines on mission fuel burn for a tiltwing transport aircraft," in *Proc. 12th AIAA Aviation Technol., Integr., Oper. (ATIO) Conf. 14th AIAA/ISSMO Multidisciplinary Anal. Optim. Conf.*, Sep. 2012, p. 5587.

[38] J. Zamboni, R. Vos, M. Emeneth, and A. Schneegans, "A method for the conceptual design of hybrid electric aircraft," in *Proc. AIAA Scitech Forum*, Jan. 2019, p. 1587.

[39] S. Kulandaivalu and Y. Sulaiman, "Recent advances in layer-by-layer assembled conducting polymer based composites for supercapacitors," *Energies*, vol. 12, no. 11, p. 2107, Jun. 2019.

[40] P. C. Vratny, H. Kuhn, and M. Hornung, "Influences of voltage variations on electric power architectures for hybrid electric aircraft," *CEAS Aeronaut. J.*, vol. 8, no. 1, pp. 31–43, Mar. 2017.

[41] G. Avanzini, A. Carlà, and T. Donateo, "Parametric analysis of a hybrid power system for rotorcraft emergency landing sequence," *Proc. Inst. Mech. Eng. G, J. Aerosp. Eng.*, vol. 231, no. 12, pp. 2282–2294, Oct. 2017.

[42] Scientific American. (Mar. 2023). *The All-New Amprius 500 Wh/kg Battery Platform is Here*. [Online]. Available: https://amprius.com/the-all-new-amprius-500-wh-kg-battery-platform-is-here/

[43] F. Salucci, "Design of electric-powered aircraft for commercial transportation," Ph.D. dissertation, Polytech. Milan, Milan, Italy, 2021.

[44] J. Hoelzen et al., "Conceptual design of operation strategies for hybrid electric aircraft," *Energies*, vol. 11, no. 1, p. 217, Jan. 2018.

[45] J. Welstead and J. L. Felder, "Conceptual design of a single-aisle turboelectric commercial transport with fuselage boundary layer ingestion," in *Proc. 54th AIAA Aerosp. Sci. Meeting*, Jan. 2016, p. 1027.

[46] R. Radebaugh, "Cryocoolers for aircraft superconducting generators and motors," *AIP Conf. Proc.*, vol. 1434, no. 1, pp. 171–182, 2012.

[47] M. D. Maisel, "NASA/Army XV-15 tilt rotor research aircraft familiarization document," Ames Res. Center, NASA, Washington, DC, USA, Tech. Rep. TM-X62, 1975.

[48] F. Nannoni, G. Giancamilli, and M. Cicale, "ERICA: The European advanced tiltrotor," in *Proc. 27th Eur. Rotorcraft Forum*, 2001, pp. 1–15.

[49] (Apr. 2014). *AW1152 AW609 Autorotation Trials Completion*. [Online]. Available: https://www.leonardo.com/en/press-release-detail/-/detail//aw609-autorotation-trials-completion

[50] D. Marten, J. Wendler, G. Pechlivanoglou, C. N. Nayeri, and C. O. Paschereit, "QBLADE: An open source tool for design and simulation of horizontal and vertical axis wind turbines," *Int. J. Emerg. Technol. Adv. Eng.*, vol. 3, no. 3, pp. 264–269, 2013.

[51] R. Prouty, "Should we consider variable rotor speeds?" *Vertiflite*, vol. 50, pp. 24–27, Dec. 2004.

[52] W. Johnson, *Helicopter Theory*. Chelmsford, MA, USA: Courier Corporation, 2012.

[53] M. D. Maisel, *The History of the XV-15 Tilt Rotor Research Aircraft: From Concept to Flight*. Washington, DC, USA: National Aeronautics and Space Administration, Office of Policy and Plans, 2000, no. 17.

Open Access funding provided by 'Università degli Studi Roma Tre' within the CRUI CARE Agreement